Published in final edited form as:

Am J Med Genet A. 2016 December ; 170(12): 3106–3114. doi:10.1002/ajmg.a.37929.

Phenotypic Evolution of UNC80 Loss of Function

Elise Valkanas[1], **Katherine Schaffer**[1], **Christopher Dunham**[2], **Valerie Maduro**[1], **Christèle du Souich**[3,4], **Rosemarie Rupps**[3,4], **David R. Adams**[1], **Alireza Baradaran-Heravi**[3,4], **Elise Flynn**[1], **May C. Malicdan**[1], **William A. Gahl**[1,5], **Camilo Toro**[1], and **Cornelius F. Boerkoel**[1,3,4]

[1]NIH Undiagnosed Diseases Program, Common Fund, Office of the Director, NIH, National Institutes of Health, Bethesda, MD, USA

[2]Department of Pathology and Laboratory Medicine, University of British Columbia, Vancouver, BC, Canada

[3]Department of Medical Genetics, University of British Columbia, Vancouver, BC, Canada

[4]Child and Family Research Institute, University of British Columbia, Vancouver, BC, Canada

[5]NHGRI, National Institutes of Health, Bethesda, MD USA

Abstract

Failure to thrive arises as a complication of a heterogeneous group of disorders. We describe two female siblings with spastic paraplegia and global developmental delay but also, atypically for the HSPs, poor weight gain classified as failure to thrive. After extensive clinical and biochemical investigations failed to identify the etiology, we used exome sequencing to identify biallelic *UNC80* mutations (NM_032504.1:c.[3983-3_3994delinsA];[2431C>T]. The paternally inherited NM_032504.1:c.3983-3_3994delinsA is predicted to encode p.Ser1328Argfs*19 and the maternally inherited NM_032504.1:c.2431C>T is predicted to encode p.Arg811*. No UNC80 mRNA was detectable in patient cultured skin fibroblasts, suggesting UNC80 loss of function by nonsense mediated mRNA decay. Further supporting the *UNC80* mutations as causative of these siblings disorder, biallelic mutations in *UNC80* have recently been described among individuals with an overlapping phenotype. This report expands the disease spectrum associated with *UNC80* mutations.

Keywords

Intellectual disability; growth restriction; failure to thrive; seizures; emaciation

Corresponding author: Cornelius F. Boerkoel, M.D., Ph.D., University of British Columbia, Department of Medical Genetics, Children's and Women's Health Centre of BC, 4500 Oak St., Rm., C234, Vancouver, B.C. V6H 3N1, Canada, Phone: 604-875-2157, Fax: 604-875-2376, cboerkoel@gmail.com.

COMPETING INTERESTS

There are no conflicts of interest to declare.

INTRODUCTION

Failure to thrive (FTT) results from inadequate calories for metabolic needs and growth. This can arise from insufficient caloric intake, malabsorption, or increased metabolism. Approximately 1–5% of infants and toddlers have feeding problems sufficiently severe to cause failure to thrive [Chatoor, 2009], and patients with neurological impairments or developmental handicaps are at particularly high risk [Aldridge et al., 2010; Schadler et al., 2007]. FTT due to poor food intake generally causes weight to fall first and spares the length and head circumference, whereas a symmetric fall in weight and height often suggests a chronic disorder.

Besides psychosocial and economic issues, problems with many organ systems can cause or contribute to FTT [Gahagan, 2006; Jaffe, 2011; Rybak, 2015; Zenel, 1997]. Such problems can include poor appetite, difficulty with ingestion, vomiting, malabsorption, and diarrhea. Problems contributing to lack of appetite include anemia, central nervous system (CNS) pathology, chronic infection, and gastrointestinal disorders. Difficulties with ingestion arise from CNS disorders, craniofacial anomalies, dyspnea, muscle weakness, gastrointestinal malformations, and as a consequence of genetic and teratogenic disorders. Causes of chronic vomiting include CNS pathology, gastrointestinal obstruction, gastroesophageal reflux, and medications. Factors contributing to malabsorption can include liver disease, food intolerance, enzyme deficiencies, immunodeficiency, and inflammatory bowel disease. Contributors to diarrhea include malabsorption, bacterial and parasitic infection, and starvation.

Herein we report two sisters who have biallelic *UNC80* loss of function mutations associated with poor weight gain and neurological impairments. Extensive imaging as well as a neurological autopsy did not identify anatomical anomalies accounting for the phenotype; this led us to hypothesize that the neurological problems are functional and not developmental.

CLINICAL REPORTS

Patient 1

The proposita (II-1 in Fig. 1A) was born to non-consanguineous parents of European descent. Family history was negative for intellectual disability, multiple congenital anomalies and recurrent miscarriages. Following an uneventful pregnancy with normal fetal movements, the proposita was born at 40 weeks gestation via induction. Her birth weight, length and head circumference were 3.149 kg (−0.18SD), 51 cm (+0.99SD), and 33 cm (−0.74SD), respectively. She was not dysmorphic (Fig. 1B). Although she did not cry immediately and was described as sleepy and lethargic, her Apgar scores were 8 and 9 at 1 and 5 minutes, respectively. She required NG tube feedings for the first 4 days, and continued to be lethargic and needed to be woken up for feeds. She has had poor weight gain throughout life (Fig. S1).

By 2 months of age, she developed alternating esotropia, poor visual fixation, truncal hypotonia, upper and lower extremity hypertonia and a high-pitched cry. She also had

myoclonic jerks and jerky movements of her extremities. Her weight, height and head circumference were 4.6 kg (−1.57SD), 51 cm (−3.81 SD) and 39.2 cm (+0.06SD), respectively. A head CT scan detected no anatomical anomalies. An EEG showed excessively slow background without epileptiform activity. She was diagnosed with cerebral palsy.

Despite intervention, her weight gain continued to fall off, and she was diagnosed with failure to thrive (Fig. 1C, D and Fig. S1). She rolled over at age 6 months, sat unsupported at 1 year. A follow-up EEG at 14 months showed a slow dysrhythmic background compatible with a seizure predisposition and diffuse cerebral dysfunction. A brain MRI at 18 months of age showed normal anatomy and myelination. In the ensuing months, she demonstrated a happy disposition, low truncal muscle tone and distal hypertonia as well as a myopathic facial appearance, a tented upper lip, a high arched palate, micrognathia, prominent finger pads and mild fifth toe clinodactyly (Fig. 1E–G).

At age 4 years and 1 month, a developmental assessment defined her overall functioning at no more than a 12-month-old equivalent; she was not autistic. At age 6 years and 11 months (Fig. 1H, I), she manifested sparse hair (trichotillomania), hooded eyelids, high arched palate, thin long face and mild micrognathia.

At age 12 years, she walked with the support of splints. Her height, weight and head circumference were 127 cm (−3.64 SD), 22.6 kg (−4.06 SD), and 52 cm (−0.94SD), respectively. Her features included dolicocephaly, hooded eyelids, intermittently disconjugate gaze, sparse hair, high palate and crowded dentition (Fig. 1J, K). Developmental assessment documented behavioral difficulties including repetitive and self-stimulatory behaviors, sensory issues such as repetitively rubbing her hands on the floor and/or licking them and mouthing objects, rigidity, communication deficits, difficulties with emotional regulation and aggression when frustrated. Her aggression included the self-injurious behaviors of dermatillomania, biting and trichotillomania. She communicated with a few words, signs, gestures and a picture exchange communication system (PECS). She developed menses at age 13 years.

Patient 2

The proposita’s sister (II-3 in Fig. 1A) had a similar history of failure to thrive, developmental delay, neurological findings and dysmorphisms. She was born following an uneventful pregnancy via elective caesarean section at 39 weeks of gestation. Her birth weight was 2.78 kg (−1.03SD). Aside from a tented upper lip, simple ears and a high arched palate, she was not dysmorphic (Fig. 1L). She was hypotonic and had a G-tube placed for poor feeding.

At age 5 weeks, she was diagnosed with focal seizures that were effectively treated with anticonvulsants. Her height, weight and head circumference were 49 cm (−2.83 SD), 3.3 kg (−2.16SD) and 35.8 cm (−1.04SD), respectively (Fig. S1). She had severe hypotonia with minimal extremity movement.

Despite intervention, her growth continued to fall off (Fig. S1), and by 10 months of age, her height, weight and head circumference were 63.5 cm (−3.26 SD), 5.5 kg (−3.69 SD) and 43 cm (−0.93SD), respectively. She fixed and followed, smiled, cooed and babbled but could not hold toys and had difficulty lifting her head; she functioned as a 4–5 month old. She had hypotonia and brisk deep tendon reflexes but no clonus. She was diagnosed with failure to thrive.

She had multiple imaging studies at age 4 years. Radiographs of the spine revealed a convex left scoliosis (55 degrees) between T5 and L3. A brain MRI detected normal myelination and no malformations.

At age 5 years (Fig. 1N), her weight and height were 12.85 kg (−3.52 SD) and 105.4 cm (−1.28SD). She was nonverbal and could not sit unsupported or walk. An abdominal ultrasound identified no anomalies suggestive of an etiology for her persistent failure to thrive (Fig. 1O, P).

At 7 years (Fig. 1Q), she presented with dehydration, respiratory distress and hypoglycemia. She had an adenoviral infection, acute liver failure, increased seizures and decreased consciousness. Her neurological status deteriorated, and she died from respiratory distress.

Results of additional investigations

Patient 1—Normal genetic investigations included a karyotype (550 band resolution), subtelomeric FISH, methylation studies of *SNRPN*, sequence analysis of *UBE3A*, and *DMPK* repeat analysis. Normal metabolic tests included transferrin isoelectric focussing, CSF amino acids and neurotransmitters, plasma amino acids, urine organic acids, urine purines and pyrimidines, serum acylcarnitines, blood ammonia and blood lactate. She also had normal audiological testing.

Patient 2—Normal genetic investigations included a karyotype (500–550 band resolution), FISH for 5p15.2 (cri-du-chat syndrome), chromosomal microarray (Affymetrix GeneChip• Human Mapping 500K Array Set), sequencing and MLPA studies of *MECP2*, *DMPK* repeat analysis, and *SNRPN* methylation. She also had random X-inactivation. Normal metabolic tests included plasma amino acids, CSF amino acids, CSF neurotransmitters, homocysteine, biotinidase, transferrin isoelectric focusing, acylcarnitine profile, urine organic acids, urine purines and pyrimidines, and blood lactate. Also, retinal and auditory examinations detected no anomalies. Multiple EEGs were abnormal consistent with predominantly grey matter involvement of both hemispheres.

METHODS

Human subjects

The individuals or guardians of the individuals participating in this study gave written, informed consent as part of a clinical protocol (76-HG-0238) approved by the Institutional Review Board of the National Human Genome Research Institute.

Nucleic acid extraction

Genomic DNA was extracted from peripheral whole blood using the Gentra Puregene Blood kit (Qiagen, Valencia, CA) per the manufacturer's protocol. Total RNA was extracted from cultured skin fibroblasts using the RNeasy Mini Kit (Qiagen, Valencia, CA) per the manufacturer's protocol. Total RNA from patient and control peripheral whole blood samples was purified using the QuickGene 810 automated extraction machine (Autogen, Holliston, MA) with an on column DNase digestion. The quality and quantity of RNA were verified using an Agilent 2100 Bioanalyzer (Agilent Technologies, Santa Clara, CA) and NanoDrop 8000 (Thermo Scientific, Waltham, MA).

SNP Chip Analysis

The Illumina GenomeStudio™ software (V2011.1, Illumina, San Diego, CA) was used to define the population frequency of the B allele (PFB) statistics for 662 samples from unrelated Undiagnosed Diseases Program (UDP) individuals. Samples were run on the Illumina Human OmniExpressExome-8v1-1_B chip and the resulting PFB file was filtered to remove mitochondrial and unanchored (chromosomal 0) SNP data. Post-filtering, GenTrain score (clustering algorithm score), genotype, B Allele Frequency (BAF), and log R Ratio (LRR) for the propositae were generated and exported. The propositae input file was run against the filtered PFB file using PennCNV [Wang et al., 2007] with thresholds of 2, 5, or 10 minimum SNPs to generate specific copy number variant (CNV) calls.

All CNV calls were manually inspected and validated for accuracy. Each copy number (CN) call position was entered into the Illumina Genome Viewer (GenomeStudio™) and manually inspected with BAF and LRR plots for each family member. Call authenticity was verified by comparing normalized intensity of the A and B allele Cartesian coordinates of the affected individuals to rest of population in the dataset. Illumina GenomeStudio™ Genotyping Module generated normalized intensity values.

A fully automatic method was used to perform Illumina GenomeStudio™ linkage exclusion based on Boolean filtration of patient genotypes [Markello et al., 2012]. Nuclear family's Illumina GenomeStudio™ formatted SNP-chip data was used to construct a BED file containing regions that segregate with disease.

Exome sequencing

Genomic DNA was extracted from peripheral whole blood of the two affected individuals, their unaffected parents, and one unaffected sibling using the Gentra Puregene Blood Kit (Qiagen, Valencia, CA). The DNA of all family members was subjected to an integrated set of genomic analyses including high-density single-nucleotide polymorphism (SNP) arrays and whole exome sequencing (WES). WES was performed on the nuclear family using the Illumina HiSeq2000 platform and the TrueSeq capture kit (Illumina, San Diego, CA). Sample library preparation, sequencing, and analysis were performed using the standard NIH Intramural Sequencing Center (NISC) pipeline. Following generation of 101 bp paired-end reads, sequence data were aligned with Novoalign using a custom alignment strategy, DiploidAlign.

This custom alignment strategy was developed to create a reference sequence for alignment that more closely resembles a patient's true genomic sequence. Phased SNP information from patient arrays as well as information from 1000 Genomes haploblock data were used to modify the standard reference sequence in to create three reference sequences for alignment: one with maternal variation, paternal information, and a third, concatenated reference.

All short reads were separately aligned to each of the three reference sequences using Novoalign (Novocraft Technologies, Selangor, Malaysia). We then used a custom extension of Picard's Liftover Java class to resolve positions and MAPQ scores between the three reference sequences, translate coordinates to hs37d5, and correct CIGAR strings. Following alignment, the single alignment was processed and variant called according to GATK's Best Practices. Samples were processed using Picard's MarkDuplicates from the Picard suite as well as Indel Realignment and Base Recalibration from GATK. Variant were called in processed alignments using the Genome Analysis Toolkit version 3.1.7 Best Practices.

Variants listed in the Variant Call Files (VCFs) were filtered based on rarity, Mendelian segregation, and predicted deleteriousness. Locations were only filtered only if an adequate number of individuals had genotype calls at the position (50 individuals in the founder cohort and 100 in ESP and 1000 Genomes). Allele frequencies were required to be < 0.05 for within the sequence data from independent individuals sequenced by the NIH UDP and < 0.02 for the Exome Sequencing Project v.0.0.20 African Ancestry population, Exome Sequencing Project v.0.0.20 European Ancestry population, and 1000 Genomes project. Also, homozygous and *de novo* variants were required to occur in < 2 individuals in the UDP founder cohort. Variants passed filtration only if they segregated with autosomal recessive, X-linked recessive, or *de novo* dominant modes of inheritance. Passing variants were required to occur within 20 bp of a splice site or have one of the following transcript effect annotations from SNPEff 3.5: frameshift, non-synonymous coding, non-synonymous stop, rare amino acid, stop lost, stop gained, splice site acceptor, splice site donor, or splice site region. Genomic search space was limited to the regions in the segregation bed file constructed during SNP array analysis. Variants that passed filtration were ranked using Exomiser 2.0 (http://www.sanger.ac.uk/resources/databases/exomiser/query/exomiser2); the shared, positive Human Phenotype Ontology terms of the patients were used as the phenotype input for Exomiser [Bone et al., 2015]. Using the Integrative Genome Viewer (https://www.broadinstitute.org/igv/home), we assessed the quality of alignment and genotype call of variants.

PCR amplification

Genomic DNA sequences of interest were amplified by polymerase chain reaction using the listed primers (Table SI), genomic DNA, and Qiagen HotStar Plus Taq polymerase under conditions: 95°C × 5 min denaturation followed by 40 cycles of 95°C × 30 s, 55°C × 30 s, 72°C × 30 s.

Sanger sequencing

Residual primers and nucleotides were removed by incubation with ExoSAP-IT (USB, Cleveland, OH). The amplicons were sequenced by Macrogen (Rockville, MD) using

BigDye terminator chemistry and compared to the human reference sequence (NCBI 37/hg19) using Sequencher (GeneCodes, Ann Arbor, MI).

Tissue Culture

Skin fibroblasts were obtained by skin biopsy from individual II-3. Unaffected, age-matched control fibroblasts were obtained from ATCC. Both affected and unaffected control fibroblasts were grown in high-glucose DMEM medium with L-glutamine (Life Technologies, Carlsbad, CA) supplemented with 10% fetal bovine serum and 1% Antibiotic-Antimycotic (Life Technologies, Carlsbad, CA). Cultured fibroblasts were incubated in a humidity –controlled environment at 37°C, with 95% O_2 and 5% CO_2. The medium was exchanged every 3 days, and the cells were used before passage 10.

Reverse Transcription Polymerase Chain Reaction and Quantitative Real-Time Polymerase Chain Reaction

Complementary DNA (cDNA) synthesis from cultured fibroblasts was performed on 2 μg of total RNA using the OminScript RT Synthesis kit (Qiagen, Valencia, CA) and Oligo dT_{23} Anchored Primers (Sigma, St. Louis, MO).

Quantitative real-time PCR was performed on 100ng of cDNA and UNC80 TaqMan Assay Hs00699496_m1, GAPDH TaqMan Assay Hs03929097_g1, and TaqMan Gene Expression Mastermix (Life Technologies, Carlsbad, CA). The reaction was analyzed with the ABI 7500 Fast Real-Time PCR System (Applied Biosystems, Foster City, CA) using standard conditions. Target amplification was normalized to that of GAPDH and shown as expression relative to control.

RESULTS

Genetic studies identify biallelic UNC80 mutations as causative of the disorder

In the absence of biochemical abnormalities or clinical features pathognomonic of a known disease, we pursued SNP array sequencing and exome sequencing of the nuclear family (Figure 1A). As observed with the clinical oligoarray, no CNVs segregated with disease based on SNP array analysis. Selection of rare exome sequencing variants segregating with disease identified variants in 4 genes meeting frequency and predicted deleteriousness requirements (Table SII). These included a pair of *UNC80* variants: paternally inherited NM_032504.1:c.3983-3_3994delinsA and maternally inherited NM_032504.1:c.2431C>T (Fig. 2A–D).

The UNC80 mutations were prioritized by Exomiser based on 1) the predicted pathogenicity of the *UNC80* mutations (Variant Score, Table SII), and 2) on the phenotypes associated with mutation of *UNC79* and *NACLN*, which encode proteins that interact with the UNC80 protein (Table I and Fig. 3; Phenotype Score, Table SII) [Al-Sayed et al., 2013; Koroglu et al., 2013; Lu et al., 2010]. To score proximity to a candidate gene, Exomiser used a random walk method previously optimized for candidate gene identification [Kohler et al., 2008; Smedley et al., 2014]. Consequently the final phenotypic relevance score was the maximum score of the comparisons between the disease/patient phenotypes and the human, mouse, or

fish annotations for the UNC80 neighbors in the interactome [Bone et al., 2015]. Recent publications of human disease associated with *UNC80* mutations affirm this Exomiser prioritization [Perez et al., 2015; Shamseldin et al., 2016; Stray-Pedersen et al., 2016].

The paternally inherited NM_032504.1:c.3983-3_3994delinsA is predicted to encode p.Ser1328Argfs*19 and the maternally inherited NM_032504.1:c.2431C>T is predicted to encode p.Arg811*. To test if these mutations cause nonsense mediated mRNA decay and thereby lead to loss of UNC80 function, we used cultured skin fibroblasts from individual II-3 to measure *UNC80* mRNA levels by qRT-PCR. Following normalization to *GAPDH* mRNA abundance, the cultured fibroblasts from individual II-3 had no detectable *UNC80* mRNA (Fig. 2E).

Post-mortem neuropathology did not detect anomalies attributable to the underlying disorder

Post-mortem neuropathological analysis of individual II-3 revealed abnormalities including bilateral subacute striatal degeneration, meningoencephalitis and thalamic perivascular/parenchymal lymphocytes and microglial nodules. The first finding is consistent with her clinical hepatic disease and “hepatic encephalopathy”. The last two findings were suggestive of a viral infection; however, PCR studies for numerous viruses were negative. There was no evidence of central nervous malformations or findings attributable to the underlying neurological disorder including those typical of many HSPs: corticospinal degeneration in the spinal cord, degeneration in the posterior columns and spinocerebellar tracts, loss of Purkinje cells and degeneration of the dentate nuclei in the cerebellum, and motor neuron pathology in the spinal cord and brain.

The post-mortem examination also identified changes in the liver and heart. The hepatic changes were hemorrhage, hepatocyte atrophy and fibrosis in the periventricular region; a finding observed with ischemic damage. The cardiac changes were epicardial fat infiltrating the right ventricular myocardium; an observation consistent with the impaired mobility of individuals with neuromuscular disorders, rather than arrythmogenic right ventricular dysplasia.

DISCUSSION

We report the longitudinal history of sisters with severe failure to thrive secondary to biallelic *UNC80* loss of function mutations. The loss of functional UNC80 did not cause neuroanatomical anomalies detectable by imaging or postmortem analyses. Lastly, implication of the *UNC80* mutations as causative variants by Exomiser prior to association of *UNC80* with human disease supports prioritizing putative causative variants based on phenotypes associated with mutation of orthologues in model organisms and on phenotypes associated with mutation of interacting proteins.

Recent association of biallelic *UNC80* [MIM: 612636] mutations with human disease have included 1) autosomal-recessive infantile encephalopathy [Shamseldin et al., 2016], 2) persistent hypotonia, encephalopathy, growth retardation, and severe intellectual disability [Stray-Pedersen et al., 2016], and 3) hypotonia, severe intellectual disability, dyskinesia and

dysmorphism [Perez et al., 2015]. The individuals described in these reports share many features with our patients (Table II).

The UNC80 homologs were identified in *C. elegans* during a screen for mutants that reverse the phenotype observed in worms with gain-of-function mutations in nca, the ortholog of NALCN [Yeh et al., 2008]. Nematodes carrying gain-of-function nca mutants have a "coiler" phenotype, i.e., exaggerated body bends and this coiler phenotype is suppressed by recessive loss-of-function mutations in unc-79 and unc-80. Additionally, nematodes with biallelic recessive loss-of-function mutations in unc-80, as well as with biallelic mutations of both nca and unc-80 recapitulate the nca loss of function phenotype. These findings suggest that nca and unc-80 act in the same pathway. Supporting this, deficiency of either nca or unc-80 protein leads to deficiency of the other [Yeh et al., 2008]. Study of the corresponding fruit fly orthologs has given similar results [Lear et al., 2013].

UNC80, NACLN and *UNC79* homologs encode proteins that form a channel complex [Lu et al., 2010]. UNC80 bridges NALCN to UNC79, and the presence of UNC80 and UNC79 are essential for channel function [Cochet-Bissuel et al., 2014; Lear et al., 2013; Lu et al., 2010]. NALCN, which has 24-transmembrane domains and is predominantly expressed in the brain, is a voltage-insensitive and nonselective sodium leak channel [Lu et al., 2007; Snutch and Monteil, 2007; Yu et al., 2005]. In cultured hippocampal neurons, it contributes to Na^+ leak at voltages close to the resting membrane potential, and extracellular Ca^{2+} regulates neuronal excitability by controlling the NALCN-dependent Na^+-leak current. The coupling between extracellular Ca^{2+} and NALCN occurs via a G protein-coupled receptor and requires the intracellular carboxy-terminus of NALCN.

Individuals with recessive biallelic amorphic mutations of NALCN manifest infantile hypotonia with psychomotor retardation and a characteristic facies (OMIM 615419) [Al-Sayed et al., 2013; Koroglu et al., 2013], and individuals with heterozygous antimorphic mutations of NALCN manifest congenital contractures of the limbs and face, hypotonia, and developmental delay (OMIM 611549) [Chong et al., 2015]. Consistent with a neurological function for the NACLN complex, mice with a targeted disruption in *Nalcn* have severely disrupted respiratory rhythms and die within 24 hours of birth [Lu et al., 2007]. Mutations in the *NALCN* homologues in *Drosophila melanogaster* (*Na*) and *Caenorhabditis elegans* (*Nca*) lead to defects in locomotion, anesthetic sensitivity, rhythmic behaviors, and synaptic function [Humphrey et al., 2007; Jospin et al., 2007; Pierce-Shimomura et al., 2008; Yeh et al., 2008].

The similarity of the neurological phenotypes of worms, fruit flies, mice and humans with mutations of UNC79-UNC80-NALCN orthologs provides *in vivo* evidence of the interdependency of the UNC79-UNC80-NALCN protein complex and conservation of function [Al-Sayed et al., 2013; Koroglu et al., 2013; Lear et al., 2013; Lu et al., 2007; Perez et al., 2015; Shamseldin et al., 2016; Speca et al., 2010; Stray-Pedersen et al., 2016; Yeh et al., 2008]. It is this evidence that was used by Exomiser in conjunction with the phenotype data to prioritize the *UNC80* mutations prior to association of *UNC80* mutations with human disease [Bone et al., 2015].

Supplementary Material

Refer to Web version on PubMed Central for supplementary material.

Acknowledgments

The authors thank the family for photographs of the propositae. This work was supported in part by the Intramural Research Program of the National Human Genome Research Institute and the Common Fund, Office of the Director (NIH, Bethesda, Maryland). This work was also supported in part by the Scottish Rite Foundation (C.D.S.) and a Child and Family Research Institute Establishment Award (C.F.B.).

References

Al-Sayed MD, Al-Zaidan H, Albakheet A, Hakami H, Kenana R, Al-Yafee Y, Al-Dosary M, Qari A, Al-Sheddi T, Al-Muheiza M, Al-Qubbaj W, Lakmache Y, Al-Hindi H, Ghaziuddin M, Colak D, Kaya N. Mutations in NALCN cause an autosomal-recessive syndrome with severe hypotonia, speech impairment, and cognitive delay. Am J Hum Genet. 2013; 93(4):721–726. [PubMed: 24075186]

Aldridge VK, Dovey TM, Martin CI, Meyer C. Identifying clinically relevant feeding problems and disorders. J Child Health Care. 2010; 14(3):261–270. [PubMed: 20534637]

Bone WP, Washington NL, Buske OJ, Adams DR, Davis J, Draper D, Flynn ED, Girdea M, Godfrey R, Golas G, Groden C, Jacobsen J, Kohler S, Lee EM, Links AE, Markello TC, Mungall CJ, Nehrebecky M, Robinson PN, Sincan M, Soldatos AG, Tifft CJ, Toro C, Trang H, Valkanas E, Vasilevsky N, Wahl C, Wolfe LA, Boerkoel CF, Brudno M, Haendel MA, Gahl WA, Smedley D. Computational evaluation of exome sequence data using human and model organism phenotypes improves diagnostic efficiency. Genet Med. 2015

Chatoor, I. Diagnosis and Treatment of Feeding Disorders in Infants, Toddlers, and Young Children. Washington: National Center for Clinical Infant Programs; 2009.

Chong JX, McMillin MJ, Shively KM, Beck AE, Marvin CT, Armenteros JR, Buckingham KJ, Nkinsi NT, Boyle EA, Berry MN, Bocian M, Foulds N, Uzielli ML, Haldeman-Englert C, Hennekam RC, Kaplan P, Kline AD, Mercer CL, Nowaczyk MJ, Klein Wassink-Ruiter JS, McPherson EW, Moreno RA, Scheuerle AE, Shashi V, Stevens CA, Carey JC, Monteil A, Lory P, Tabor HK, Smith JD, Shendure J, Nickerson DA, Bamshad MJ. University of Washington Center for Mendelian G. De novo mutations in NALCN cause a syndrome characterized by congenital contractures of the limbs and face, hypotonia, and developmental delay. Am J Hum Genet. 2015; 96(3):462–473. [PubMed: 25683120]

Cochet-Bissuel M, Lory P, Monteil A. The sodium leak channel, NALCN, in health and disease. Front Cell Neurosci. 2014; 8:132. [PubMed: 24904279]

Gahagan S. Failure to thrive: a consequence of undernutrition. Pediatr Rev. 2006; 27(1):e1–11. [PubMed: 16403734]

Humphrey JA, Hamming KS, Thacker CM, Scott RL, Sedensky MM, Snutch TP, Morgan PG, Nash HA. A putative cation channel and its novel regulator: cross-species conservation of effects on general anesthesia. Curr Biol. 2007; 17(7):624–629. [PubMed: 17350263]

Jaffe AC. Failure to thrive: current clinical concepts. Pediatr Rev. 2011; 32(3):100–107. quiz 108. [PubMed: 21364013]

Jospin M, Watanabe S, Joshi D, Young S, Hamming K, Thacker C, Snutch TP, Jorgensen EM, Schuske K. UNC-80 and the NCA ion channels contribute to endocytosis defects in synaptojanin mutants. Curr Biol. 2007; 17(18):1595–1600. [PubMed: 17825559]

Kohler S, Bauer S, Horn D, Robinson PN. Walking the interactome for prioritization of candidate disease genes. Am J Hum Genet. 2008; 82(4):949–958. [PubMed: 18371930]

Koroglu C, Seven M, Tolun A. Recessive truncating NALCN mutation in infantile neuroaxonal dystrophy with facial dysmorphism. J Med Genet. 2013; 50(8):515–520. [PubMed: 23749988]

Lear BC, Darrah EJ, Aldrich BT, Gebre S, Scott RL, Nash HA, Allada R. UNC79 and UNC80, putative auxiliary subunits of the NARROW ABDOMEN ion channel, are indispensable for robust circadian locomotor rhythms in Drosophila. PLoS One. 2013; 8(11):e78147. [PubMed: 24223770]

Lu B, Su Y, Das S, Liu J, Xia J, Ren D. The neuronal channel NALCN contributes resting sodium permeability and is required for normal respiratory rhythm. Cell. 2007; 129(2):371–383. [PubMed: 17448995]

Lu B, Zhang Q, Wang H, Wang Y, Nakayama M, Ren D. Extracellular calcium controls background current and neuronal excitability via an UNC79-UNC80-NALCN cation channel complex. Neuron. 2010; 68(3):488–499. [PubMed: 21040849]

Markello TC, Han T, Carlson-Donohoe H, Ahaghotu C, Harper U, Jones M, Chandrasekharappa S, Anikster Y, Adams DR, Program NCS, Gahl WA, Boerkoel CF. Recombination mapping using Boolean logic and high-density SNP genotyping for exome sequence filtering. Mol Genet Metab. 2012; 105(3):382–389. [PubMed: 22264778]

Perez Y, Kadir R, Volodarsky M, Noyman I, Flusser H, Shorer Z, Gradstein L, Birnbaum RY, Birk OS. UNC80 mutation causes a syndrome of hypotonia, severe intellectual disability, dyskinesia and dysmorphism, similar to that caused by mutations in its interacting cation channel NALCN. J Med Genet. 2015

Pierce-Shimomura JT, Chen BL, Mun JJ, Ho R, Sarkis R, McIntire SL. Genetic analysis of crawling and swimming locomotory patterns in C. elegans. Proc Natl Acad Sci U S A. 2008; 105(52): 20982–20987. [PubMed: 19074276]

Rybak A. Organic and Nonorganic Feeding Disorders. Ann Nutr Metab. 2015; 66(Suppl 5):16–22. [PubMed: 26226993]

Schadler G, Suss-Burghart H, Toschke AM, von Voss H, von Kries R. Feeding disorders in ex-prematures: causes--response to therapy--long term outcome. Eur J Pediatr. 2007; 166(8):803–808. [PubMed: 17120038]

Shamseldin HE, Faqeih E, Alasmari A, Zaki MS, Gleeson JG, Alkuraya FS. Mutations in UNC80, Encoding Part of the UNC79-UNC80-NALCN Channel Complex, Cause Autosomal-Recessive Severe Infantile Encephalopathy. Am J Hum Genet. 2016; 98(1):210–215. [PubMed: 26708753]

Smedley D, Kohler S, Czeschik JC, Amberger J, Bocchini C, Hamosh A, Veldboer J, Zemojtel T, Robinson PN. Walking the interactome for candidate prioritization in exome sequencing studies of Mendelian diseases. Bioinformatics. 2014; 30(22):3215–3222. [PubMed: 25078397]

Snutch TP, Monteil A. The sodium “leak” has finally been plugged. Neuron. 2007; 54(4):505–507. [PubMed: 17521564]

Speca DJ, Chihara D, Ashique AM, Bowers MS, Pierce-Shimomura JT, Lee J, Rabbee N, Speed TP, Gularte RJ, Chitwood J, Medrano JF, Liao M, Sonner JM, Eger EI 2nd, Peterson AS, McIntire SL. Conserved role of unc-79 in ethanol responses in lightweight mutant mice. PLoS Genet. 2010; 6(8)

Stray-Pedersen A, Cobben JM, Prescott TE, Lee S, Cang C, Aranda K, Ahmed S, Alders M, Gerstner T, Aslaksen K, Tetreault M, Qin W, Hartley T, Jhangiani SN, Muzny DM, Tarailo-Graovac M, van Karnebeek CD, Lupski JR, Ren D, Yoon G. Care4Rare Canada C, Baylor-Hopkins Center for Mendelian G. Biallelic Mutations in UNC80 Cause Persistent Hypotonia, Encephalopathy, Growth Retardation, and Severe Intellectual Disability. Am J Hum Genet. 2016; 98(1):202–209. [PubMed: 26708751]

Wang K, Li M, Hadley D, Liu R, Glessner J, Grant SF, Hakonarson H, Bucan M. PennCNV: an integrated hidden Markov model designed for high-resolution copy number variation detection in whole-genome SNP genotyping data. Genome Res. 2007; 17(11):1665–1674. [PubMed: 17921354]

Yeh E, Ng S, Zhang M, Bouhours M, Wang Y, Wang M, Hung W, Aoyagi K, Melnik-Martinez K, Li M, Liu F, Schafer WR, Zhen M. A putative cation channel, NCA-1, and a novel protein, UNC-80, transmit neuronal activity in C. elegans. PLoS Biol. 2008; 6(3):e55. [PubMed: 18336069]

Yu FH, Yarov-Yarovoy V, Gutman GA, Catterall WA. Overview of molecular relationships in the voltage-gated ion channel superfamily. Pharmacol Rev. 2005; 57(4):387–395. [PubMed: 16382097]

Zenel JA Jr. Failure to thrive: a general pediatrician’s perspective. Pediatr Rev. 1997; 18(11):371–378. [PubMed: 9360433]

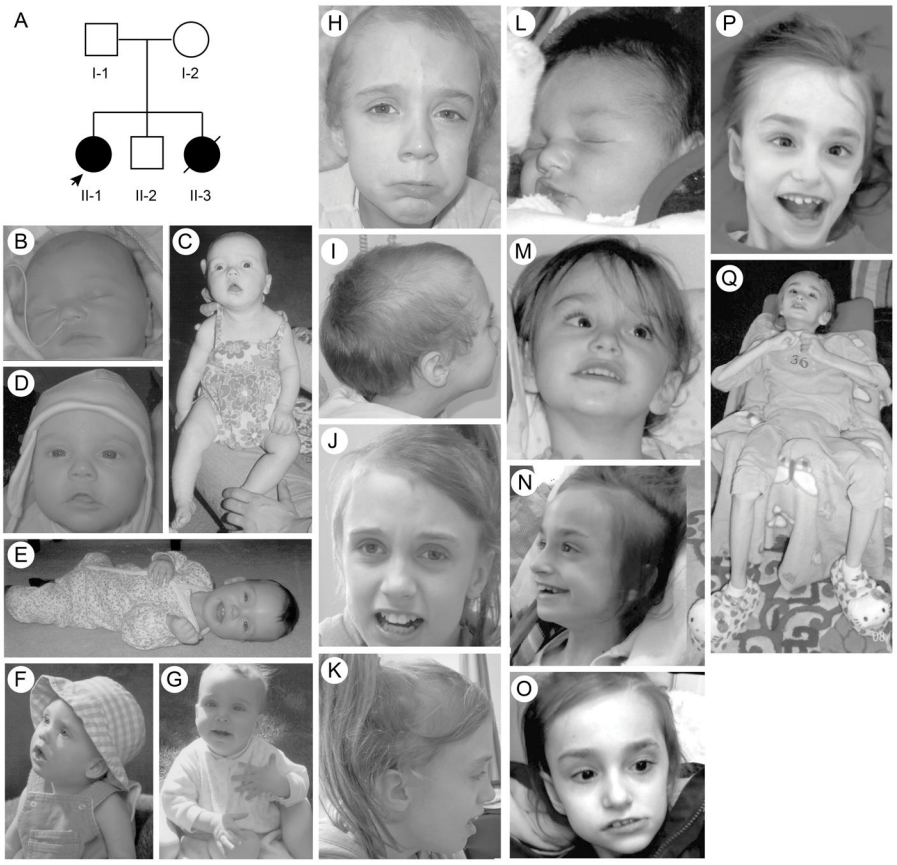

FIG. 1.

Clinical photographs of the proposita (arrow, II-1) and her affected sister (II-3). (**A**) Family pedigree. Affected individuals are shown by black symbols. (**B–K**) Photographs of the proposita at age 1 week (**B**), 4 months (**C**), 6 months (**D**), 17 months (**E**), 15 months (**F**), 19 months (**G**), 6 years and 11 months (**H, I**), and 12 years and 10 months (**J, K**). (**L–Q**) Photographs of the affected sister (II-3) of the proposita as a newborn (**L**) and at ages 2 years (**M**), 5 years (**N**), 6 years (**O, P**) and 7 years (**Q**).

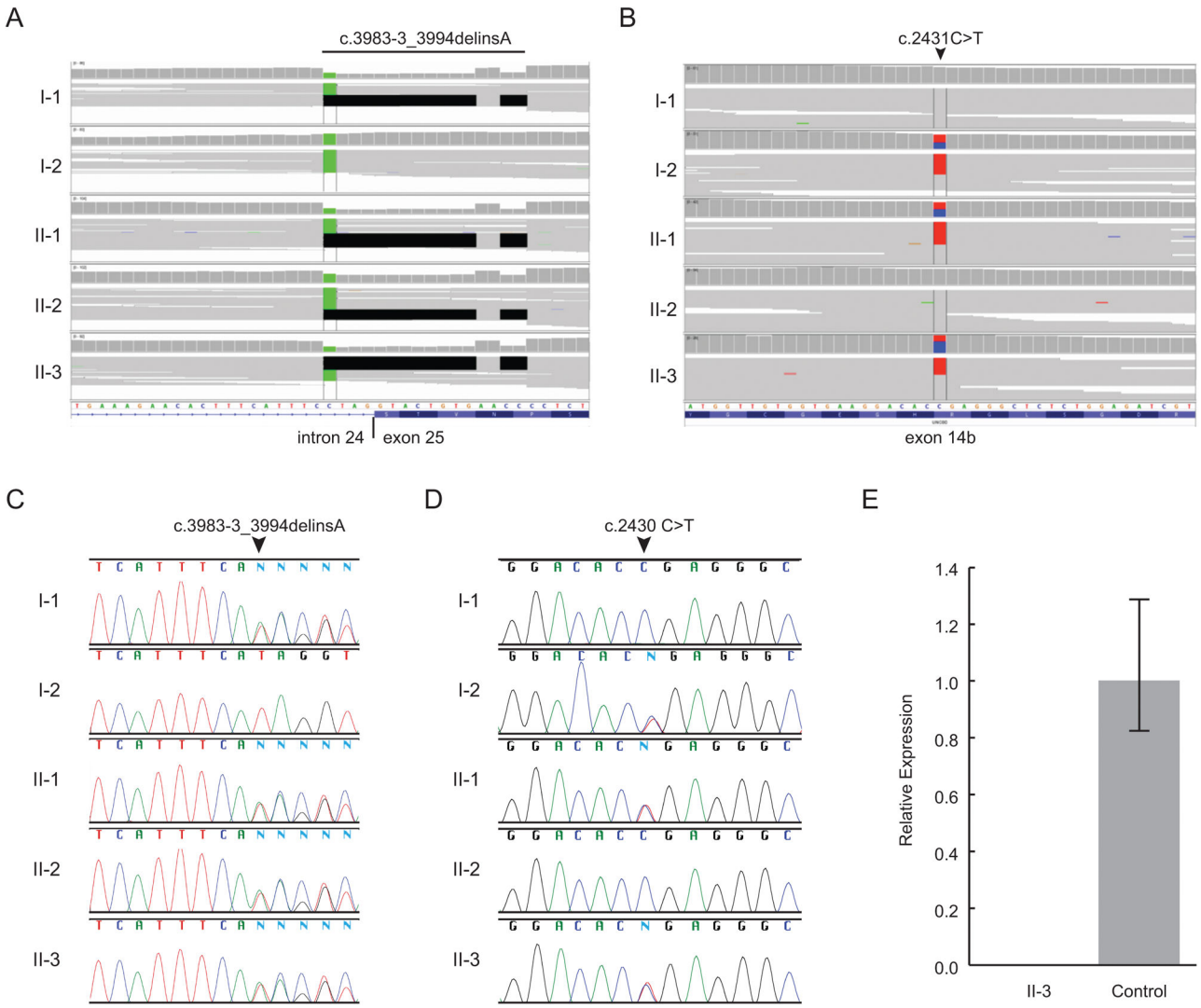

FIG. 2.

Identification and characterization of biallelic *UNC80* mutations. (A) IGV views of aligned exome sequencing short reads showing paternally inherited NM_032504.1:c.3983-3_3994delinsA. (B) IGV views of aligned exome sequencing short reads showing maternally inherited NM_032504.1:c.2431C>T. Neither mutation has been previously published. (C) Sanger traces for PCR amplification products of NM_032504.1:c.3983-3_3994delinsA. (D) Sanger traces for PCR amplification products of NM_032504.1:c.2431C>T. (E) *UNC80* qRT-PCR amplification showing the absence of detectable *UNC80* mRNA in cultured skin fibroblasts derived from patient II-3. Target amplification was normalized to that of GAPDH and shown as expression relative to control.

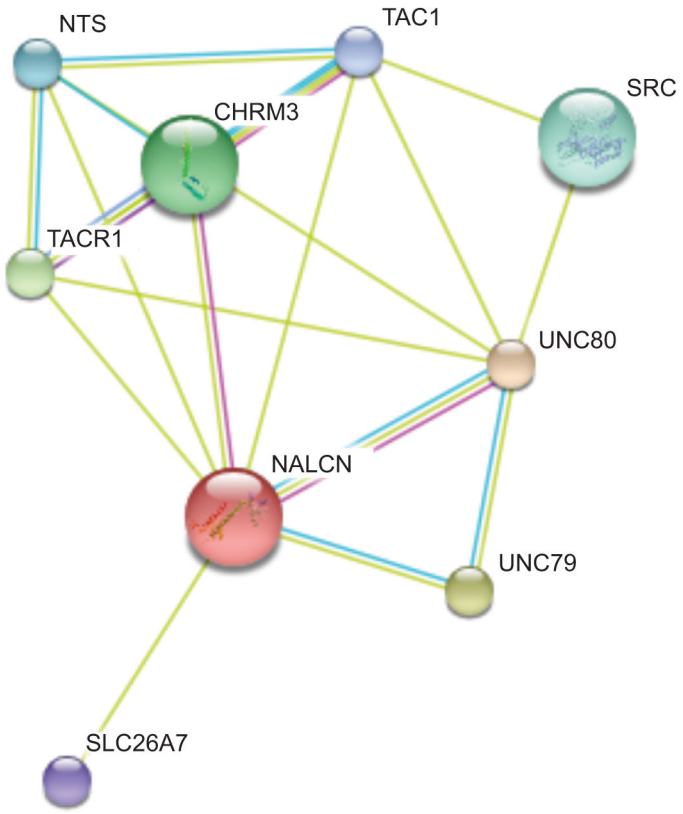

FIG 3.

STRING diagram referenced by Exomiser and showing the proximity of UNC80 in the interactome to NALCN. The edges of this diagram indicate predicted functional links and are colored to indicate supporting evidence for that link (green indicates proteins in the same neighborhood; pink indicates a connection made through experimentation; yellow connections established via text mining for co-occurrence of gene or protein names in abstracts; and light blue indicates relationships supported in databases Biocarta, BioCyc, GO, KEGG, and Reactome). Applying Exomiser to each variant that passed the frequency and segregation filters, we were able to compare the patient's HPO terms to all human diseases associated with the gene containing the variant in OMIM or Orphanet, to phenotypes associated with orthologs mutated in mice or zebrafish, and lastly to phenotypes associated with nearby genes in the protein-protein association network. For the propositae, Exomiser calculated the phenotype score by considering the similarity of their phenotype to mutation of *NACLN* (Table I) and the proximity of NACLN to UNC80. The Exomiser variant score is a measure of the predicted pathogenicity and allele frequency of a variant. Exomiser also generated a general score that was calculated from the phenotype and variant scores.

Table I

Human Phenotype Ontology terms (HP ID) of patient II-1 matched to the HP IDs associated with mutation of NACLN generated using Exomiser.

HP ID	Patient Phenotype	HP ID	Matched Phenotype
HP:0011398	Central hypotonia	HP:0002510	Spastic tetraplegia
HP:0001319	Neonatal hypotonia	HP:0008936	Muscular hypotonia of the trunk
HP:0002510	Spastic tetraplegia	HP:0002510	Spastic tetraplegia
HP:0000487	Congenital strabismus	HP:0000486	Strabismus
HP:0000565	Esotropia	HP:0000486	Strabismus
Phenotype Score: 0.539		Variant Score: 0.95	Exomiser Score: 0.739

The Exomiser Score is derived from the Phenotype and Variant Scores.

Table II

Comparison of features among individuals with *UNC80* mutations (table adapted from Perez et al., Shamseldin et al., and Stray-Pedersen et al.)

Clinical Features	Summary of reported patients			
	Perez et al., 2015 (n=7)	Shamseldin et al., 2016 (n=6)	Stray-Pedersen et al., 2016 (n=4)	Our patients (n=2)
Face[*]				
Downslanting PF	3/7	5/6	0/4	2/2
Triangular face	6/7	6/6	2/4	2/2
Frontal bossing	5/7	n/a	n/a	1/2
Low set/posteriorly rotated ears	7/7	2/5	1/3	0/2
Anteverted nasal tip	7/7	3/6	1/4	0/2
Broad nasal bridge	7/7	2/6	2/4	0/2
Large nares	4/7	3/6	0/4	0/2
Short and smooth philtrum	7/7	1/1	2/3	0/2
Micrognathia	3/7	3/6	2/4	2/2
Thin upper lip	6/7	0/5	0/4	2/2
Tented upper lip	1/2	4/6	3/3	2/2
Hands and Feet				
Long thin fingers	7/7	n/a	n/a	2/2
Tapering of distal phalanx	7/7	n/a	n/a	2/2
Club feet	4/7	n/a	n/a	2/2
Small hands and feet	n/a	n/a	3/4	2/2
Orthopedic				
Scoliosis	7/7	n/a	1/4	2/2
Contractures	7/7	1/1	n/a	2/2
Ophthalmological findings				
Strabismus	7/7	2/2	n/a	2/2
Esotropia	7/7	n/a	3/4	1/1
Nystagmus	n/a	2/2	n/a	0/2
Gastrointestinal findings				
Constipation	n/a	n/a	4/4	1/2
Feeding difficulties	n/a	n/a	3/4	2/2
Growth findings				
Normal birth parameters	n/a	6/6	4/4	2/2
Height < 3rd centile	n/a	5/6	4/4	2/2
Weight < 3rd centile	n/a	5/6	4/4	2/2
Microcephaly	7/7	3/6	1/4	0/2
Developmental findings				
Severe ID or DD	7/7	6/6	4/4	2/2
Hypotonia	7/7	6/6	4/4	2/2

Clinical Features	Summary of reported patients			
	Perez et al., 2015 (n=7)	Shamseldin et al., 2016 (n=6)	Stray-Pedersen et al., 2016 (n=4)	Our patients (n=2)
Global motor delay	7/7	n/a	4/4	2/2
Walking achieved	n/a	n/a	2/4	1/2
Absent speech or <5 words	7/7	6/6	4/4	2/2
Neurological				
Dystonic posture of limbs	7/7	n/a	n/a	2/2
Seizures	4/7	1/6	4/4	1/2
Abnormal head MRI	2/6[a]	1/4[b]	1/4[c]	0/2
Behavioural findings				
Arm flapping	n/a	n/a	n/a	2/2
Hand biting	n/a	n/a	n/a	2/2
Happy disposition	n/a	n/a	n/a	2/2
Self-injury	n/a	n/a	n/a	2/2
Sensory hypersensitivities	n/a	n/a	3/4	2/2

Abbreviations: PF, palpebral fissures

[*] CFB and CDS defined facial features in patients reported by Perez et al., Stray-Pedersen et al., and Shamseldin et al. by examining the patient photographs included in the respective papers.[Perez et al., 2015; Shamseldin et al., 2016; Stray-Pedersen et al., 2016]

[a] 2 individuals showed borderline mild enlargement of the lateral and third ventricles and of the extra-axial space

[b] one patient had a thin corpus callosum

[c] one patient had mild diffuse brain atrophy